

Restyling Data: Application to Unsupervised Domain Adaptation

Vasileios Gkitsas

Antonios Karakottas

Nikolaos Zioulis

Dimitrios Zarpalas

Petros Daras

Information Technologies Institute (ITI), Centre for Research and Technology Hellas (CERTH), Greece
 {gkitsasv, ankarako, nzioulis, zarpalas, daras}@iti.gr

Abstract

Machine learning is driven by data, yet while their availability is constantly increasing, training data require laborious, time consuming and error-prone labelling or ground truth acquisition, which in some cases is very difficult or even impossible. Recent works have resorted to synthetic data generation, but the inferior performance of models trained on synthetic data when applied to the real world, introduced the challenge of unsupervised domain adaptation. In this work we investigate an unsupervised domain adaptation technique that descends from another perspective, in order to avoid the complexity of adversarial training and cycle consistencies. We exploit the recent advances in photorealistic style transfer and take a fully data driven approach. While this concept is already implicitly formulated within the intricate objectives of domain adaptation GANs, we take an explicit approach and apply it directly as data pre-processing. The resulting technique is scalable, efficient and easy to implement, offers competitive performance to the complex state-of-the-art alternatives and can open up new pathways for domain adaptation.

1. Introduction

The proven capability of deep convolutional neural networks (CNNs) to represent complex functions has been steadily pushing their adoption in many computer vision tasks. A great deal of work focuses on boosting their performance by increasing their expressiveness through architectural modifications or richer supervision schemes. Nonetheless, for most vision related tasks, the main driving force behind deep CNNs is unarguably the amount of training data.

From a practical standpoint, their real world applicability is related to their efficacy when applied to in-the-wild settings. In other words, each CNN's capability to generalize and retain its performance in a variety of environments and conditions, is of paramount importance. There

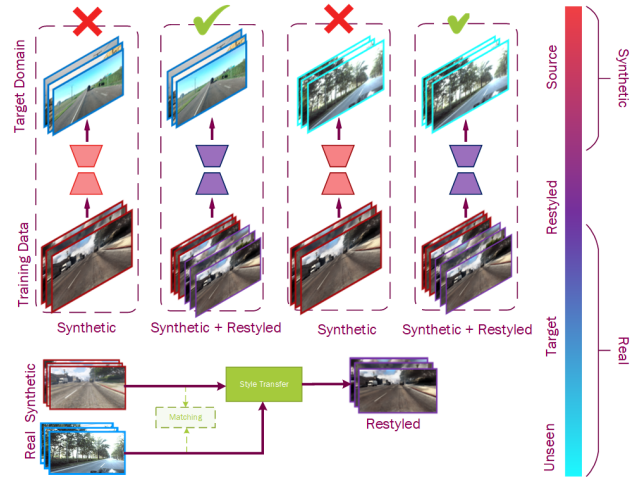


Figure 1: Overview of the proposed method. We use style transfer explicitly to align data distributions at the dataset level. Starting from a **labelled synthetic source** domain we select samples from an **unlabelled realistic target** domain and restyle them to create a **labelled restyled** domain, more aligned to the target one. This is used to enrich the original labelled dataset. Data selection can be either random or matched via perceptual hashing (Sec. 3). The enriched dataset is used to train a model that learns feature representations more aligned to the realistic target domain used to restyle the original synthetic source data. This improves its performance when applied to data from the unlabelled target domain, compared to training only with the labelled source data. Further, the model shows performance gains even when applied to **other realistic domains (unseen)** which are closer to the target domain than the source (as indicated by the domain alignment color scale on the right). Best viewed in color.

are many techniques that are being employed to address this, like dropping neurons [41] or layers [20], parameter sharing and regularization, all being different ways to prevent over-fitting. However, increasing the amount and diversity of the training data is also an indirect way to increase their generalization capacity and prevent over-fitting.

As labelled data acquisition is costly and inefficient, photo-realistic automatic data synthesis via computer graphics technologies is a promising alternative [11], with another one being data recording from computer games [33]. Nevertheless, besides the inherent dataset bias [44], such automatic data generation methods suffer from the synthetic-to-real (S2R) domain discrepancy [49] that deteriorates the performance of models trained using rendered content when applied to real world acquired inputs.

State-of-the-art S2R domain adaptation methods typically utilize Generative Adversarial Networks (GANs) [15] to align the source (synthetic) and target (real) domains under an adversarial framework. Different variants exist that operate either in the image [4, 27] or feature space [12]. However, these approaches do not generalize well to other tasks [50], leading to the development of task specific approaches [38]. Other approaches rely on image-to-image translation to create a mapping between the source and target domains [42] or employ GANs to transfer the style of the target domain to the labelled source images [3].



Figure 2: Examples showcasing the visual quality increase when matching styles randomly (RS), compared to style selection via perceptual hashing (PH). For each subfigure from top to bottom: the source image (top), the selected style (middle) and the restyled result (bottom). Uncanny effects are observed when randomly picking out the styles, compared to when using PH as the style-matching process, which improves the overall quality of the result.

GAN based approaches though, require the training of a generator-discriminator pair which is a challenging task. They also reduce the effective expressiveness and training time of the underlying model that is trained for the targeted task, as the adaptation itself consumes model capacity and training resources. In actual industrial or production settings, new and diverse data can be acquired at enormous rates, but labelling them is a tedious and labour intensive

task. The suitability of GAN based solutions in production settings is questionable, as their associated challenges would be further magnified. Therefore, novel solutions are required that are scalable and flexible.

In this work, we explore one such alternative and find it to be very promising due to its applicability. We showcase how the recent advances in direct style transfer [14] can bridge the domain gap, even when applied purely as data pre-processing. More importantly, our approach operates in an unsupervised manner as it does not require cross domain labels and, accordingly, it can readily use an abundance of unlabelled data. Our concept is illustratively presented in Figure 1. In summary our contributions are: **i)** We demonstrate a straightforward and effective technique for unsupervised domain adaptation (UDA) that offers competitive performance against the state-of-the-art, but without its complexity. **ii)** We present a sample selection process that is suitable for appropriately matching labelled samples of the source data distribution with unlabelled ones from the target data distribution, in order to improve the performance of our proposed technique. **iii)** We extensively evaluate our approach and demonstrate its generality across different tasks and datasets. **iv)** Unlike most similar approaches, we take a step beyond and consider *target* domains that - albeit contextually similar - are different from both the labelled (*source*), as well as the unlabelled (*style*) domains.

2. Related work

UDA aims at overcoming the domain shift between a *source* domain used to train a machine learning model, and the *target* domain that it will be applied to, whose data distribution differs from the source one. The lack of supervision implies that labelled data are only available for the source domain. Vision related machine learning tasks mostly rely on CNNs, and consequently, preliminary works introduced domain classifiers along with gradient reversal on their results, adding another objective for the CNN to optimize for, which ensured domain invariant feature learning [12]. Initial results were presented for digit [24] and object [36] classification, and later extended to other tasks [13]. However, the datasets used are limited by today’s standards in terms of scale and domain gap benchmarking potential.

With the introduction of the highly performing GANs [15], most of the recent UDA methods rely on adversarial objectives between the source and target data distributions. A two-fold approach was presented in [18] with global domain alignment enforced by a domain classifier, operating on the encoded representations of the source and target domains, and local domain adaptation enforced by optimizing for consistency between the category probabilities of each distribution. As this approach is driven by the assumption that both domains contain similar distributions of the categories, it is limited only to dense segmentation scenarios

While quantitative results were presented using SYNTHIA [35] and GTA [33] as source domains and Cityscapes (CS) [8] as the target domain, an in-the-wild dataset was also collected for assessing adaptation between real world environments as well. In [50], focusing on semantic segmentation, a CNN is trained with direct supervision on the source domain, as well as properties consistent with the target domain like global and local label distributions, with the latter enforced via superpixel landmarks. Results were presented for SYNTHIA and Cityscapes as the source and target domains respectively.

Other works [30, 17] approached the problem of UDA under an unpaired image-to-image translation framework. In the former [30], a complex optimization was formulated using numerous objectives that are weighted together to learn a domain agnostic feature representation for both the source and the target distributions. Overall, inter domain translations were used, along with cycle consistencies between them and translation classification losses. In the latter [17], the concept of cycle consistent adversarial networks [51] is used to produce mappings between the source and target domains. Reconstruction and discriminator losses were utilized for the $source \rightarrow target \rightarrow source$ and the $source \rightarrow target$ mappings respectively, in addition to a task specific loss for the second mapping. As both of these frameworks are generic, they were applied to the digit classification and semantic segmentation tasks.

SG-GAN [25] complements cycle consistencies and adversarial discriminators with a soft-gradient objective that aims to align texture edges with semantic boundaries, and presents results for the GTA to CS semantic segmentation task. Similarly, [38] utilizes direct supervision on the source domain, shared weights auto-encoders with an adversarial loss, to not only reconstruct but also distinguish the domains between the reconstructions, as well as an auxiliary supervision on the reconstructed image. Their provided results focus on virtual to real adaptation using the SYNTHIA and GTA datasets that are evaluated on Cityscapes. Taking a slightly more original approach, [45] chose to discriminate based on the output semantic segmentation map on multiple scales and demonstrate their method under a S2R theme using GTA and SYNTHIA adapted to CS, and also under a real-to-real scheme, using CS and a Cross-City dataset [7].

Perhaps one of the more original ideas is based on the adversarial dropout regularization concept [37] that searches for non-discriminative features on the shared encoding, and aims to achieve a better separation of the distribution at their boundaries.

More recently, the issues that traditional batch normalization creates during domain adaptation were acknowledged by [34], and then adapted this technique appropriately for domain adaptation. A two-step training process was used that involved first training a domain discrimina-

tor, and then using it to drive a confusion loss while directly supervising the source domain. Besides offering results for the GTA to CS task, they also reported performance on unseen real data, and more specifically, in Mapillary Vistas (Map) [31] and ApolloScape (AS) [21]. In [53] the novel concept of self-training is introduced, where target domain *pseudo*-labels are estimated under an iterative self-training framework with spatial priors, achieving state-of-the-art results on the S2R adaptation task on SYNTHIA and GTA to CS experiments.

An orthogonal task to UDA is style transfer [14], as the transfer of the style of a target domain to a source one, aligns with the concept of adapting a model from one domain to another. This was the driving idea behind [3] which used a GAN to learn the task of monocular depth estimation in the target domain and showcased their concept in a S2R adaptation task using GTA and KITTI [29]. Nevertheless, transferring the style of one domain to another has only been an implicit goal of some approaches while it has been explicitly used as data augmentation and partly for domain adaptation by [23, 43]. Both utilize artistic – and not photo-realistic – style transfer, for improving the network’s generalization. The former [23] investigate the effect of style augmentation on three tasks (image classification, cross-domain classification and depth estimation) whereas the latter [43] enforces the network to learn domain invariant features between source and restyled samples.

Overall, we observe a trend in using adversarial learning and cycle consistencies for UDA, as well as a focus on classification, either image-wide or at the pixel level. Further, even though these methods’ complexity is increasing, we rarely see evaluations on a wider domain spectrum, i.e. what is typically considered as “*real*” is a single dataset acquired from the real world, but the fact that there are still different “*real*” domains has not been properly addressed. Some works have lightly touched this by evaluating their performance in unseen “similar” domains [3, 34], but most works typically require re-training to properly adapt to another “*real*” domain [28].

3. Approach

The general problem of UDA considers a set of samples x_s drawn from a *source* distribution \mathcal{X}_s along with their corresponding labels y_s . For vision related tasks, the labels y_s are either on a per image basis (e.g. classes or bounding boxes) or on a per pixel basis (e.g. class labels for semantic segmentation, continuous scalar or vector values for depth or surface estimation respectively) depending on the task. In addition, a *target* distribution \mathcal{X}_t , different from \mathcal{X}_s , but similar in context, is also considered, offering a variety of unlabelled samples x_t . The goal is to train a machine learning model (CNN in the case of vision tasks) with parameters θ , in order to learn a function f , without the availability

of corresponding labelled data y_t for the target domain \mathcal{X}_t , and maximize its performance when applied to data derived from \mathcal{X}_t . Most approaches train a function $y = f(x, \theta)$ using the paired source samples x_s, y_s and then adapt the parameters θ to increase performance on the target domain.

As aforementioned, \mathcal{X}_s and \mathcal{X}_t are similar in context, thereby depicting similar content and differing only in color distribution and patterns, as well as potentially in the noise levels (this is especially true for the realistic vs synthetic domains). Driven by this, we identify a new solution to the UDA problem, based on the orthogonal style transfer concept. Style transfer focuses on transferring the *style* of one image x_{st} to the *content* of another image x_c , thereby producing a restyled image x_{re} that preserves the content representation of x_c and the style of x_{st} .

Our proposition stems from the intuition and observation that recent advances in style transfer better preserve the structure of the content image, while simultaneously transferring the appearance details of the style image. We hypothesize that by enriching the source data distribution \mathcal{X}_s with data drawn from a restyled distribution \mathcal{X}_{re} , and training f with the new data distribution $\mathcal{Z} := \mathcal{X}_s \cup \mathcal{X}_{re}$, the performance of $y_t = f(x_t, \theta)$ will increase. The restyled distribution will produce samples x_{re} that will be the result of style transfer from a set of target (style) samples x_t to a set of source (content) samples x_s . As shown in [9], data augmentations lead to feature averaging and improve generalization by inducing model invariance. Hence, we expect that our non-linear style transfer transformations will infuse the target domain’s features into the data and improve the performance of the model in the target distribution. Consequently, \mathcal{Z} will still depict the same content but it will also include the style of the target domain, enabling the learning of features aligned to both domains. An illustration of this concept can be found in Figure 1.

A naive approach would be to randomly sample (RS) the target distribution \mathcal{X}_t to find matching styles to each source sample. However, that will lead to uncanny restyles and reduce the adaptation efficiency. We propose to use the samples’ structure to enforce consistency in the matching process and facilitate more effective data restyling to improve domain alignment. Under a spatial frequency transform, the image domain can be disentangled into the main structural information and its detail layers. Naturally, low frequencies correspond to the former and comprise the image’s content, while higher frequencies composite texture onto the structure and comprise the image’s style. Therefore, after encoding all images (source and target alike) under a frequency transform and matching them using this encoding, the corresponding spatial structure information between the matches will produce visually appealing restyled results.

Accordingly, we leverage perceptual hashing (PH) [46], a technique used in reverse image search products (e.g.

Google Images), to match source and target samples. We transform samples from \mathcal{X}_s and \mathcal{X}_t using discrete cosine transform (DCT) into the frequency domain:

$$\mathcal{T} = A \times g \times A^T,$$

where \mathcal{T} represents the resulting *DCT* spectrum, A is a quadratic, real-valued, orthonormal transformation matrix, and g is a low-resolution grayscale transformed sample x . Then, we extract the low frequencies (8×8 top left block) and calculate the median value after excluding the high amplitude DC term. Subsequently, a 64-bit hash \mathcal{H} is constructed after thresholding the lowest frequencies based on the computed median value. Finally, structural matches can be established between the samples drawn from the source \mathcal{X}_s and target \mathcal{X}_t distributions, using their hashes’ Hamming distance as a matching criterion. It should be noted that unlike cryptographic hash functions, in perceptual hashing, small changes in the input will not lead to drastic changes in the output. A qualitative comparison between randomly restyling data and selecting structural matches can be seen in Figure 2, where it is apparent that matched restyles produce more plausible results when using Mapillary as the style domain.

4. Experiments

Although our proposed technique is only applicable to image data, and thus to vision related tasks, it is conceptually generic. We conduct a series of experiments in two different vision tasks to validate this, mostly focusing on S2R UDA.

We define the following notation to disambiguate each dataset’s role in the experiments: $src(stl) \rightarrow tgt$, with src referring to the source dataset, stl to the dataset that the styles are derived from, and tgt is the target dataset, i.e. the dataset used for our experimental validation.

Implementation details: For style transfer we use a photo-realistic method [26] that better preserves structural information and is faster than other approaches. We apply data restyling as a pre-processing step on a source dataset and then merge the restyled data with the source ones, and use the merged dataset for training. We first hash all source and target domain image samples and then use a brute-force nearest neighbor to match K target samples to each source image.

Our experiments were run on a single machine with an i7 processor and a NVidia Titan X GPU. Nonetheless, this technique is inherently parallel as all pre-processing steps (hashing, matching, restyling) can be run independently for each sample. While the experiments on a single machine were lengthy, the proposed technique can easily scale out to allow for faster dataset-wide pre-processing or the accommodation of very large style/target datasets. Setting out to

Table 1: Domain adaptation results on the Mapillary Vistas dataset, As with Table 3, the same applies regarding metrics and results presentation, except from ours, where the second row shows results for the configuration GTA(RS-Map) \rightarrow Map, and the third for GTA(PH-Map) \rightarrow Map.

GTA(Mapillary) \rightarrow Mapillary

Method	network	road	sidewalk	building	wall	fence	pole	t-light	t-sign	veg	terrain	sky	person	rider	car	truck	bus	train	mbike	bike	mIoU	pix.acc	mIoU gain	pix.acc.gain
UADA [34]	ResNet-50																				37.1	-		
																					38.5	-	+1.4	
Baseline	ResNet-101	48.83	19.24	59.37	6.47	12.82	13.55	14.62	13.77	64.63	10.51	89.63	35.8	13.25	43.7	21.32	7.81	1.0	22.66	18.11	27.22	72.4		
Ours-RS		72.88	24.68	66.74	14.93	17.13	15.14	19.83	26.12	72.49	16.44	92.74	37.63	9.07	71.77	33.6	12.93	0.0	25.56	19.39	34.16	81.1	+6.94	+8.7
Ours-PH		82.71	28.01	68.81	13.88	18.87	18.18	20.29	38.74	76.37	22.68	92.14	40.54	17.4	76.58	39.8	7.86	1.02	24.54	24.63	37.53	85.9	+10.31	+13.5

Table 2: Domain adaptation results on the Apolloscape dataset, showing IoU for each class, mean IoU (mIoU), pixel accuracy, mIoU gain and pixel accuracy gain.

GTA(Mapillary) \rightarrow Apolloscape

Method	network	road	sidewalk	building	wall	fence	pole	t-light	t-sign	veg	terrain	sky	person	rider	car	truck	bus	train	mbike	bike	mIoU	pix.acc	mIoU gain	pix.acc.gain
UADA [34]	ResNet-50																				25.3	-		
																					27.4	-	+2.1	
Baseline	ResNet-101	80.52	0.19	7.16	0.14	18.12	7.16	6.22	2.82	41.89	-	80.27	0.45	0.05	75.63	33.74	6.42	-	0.0	0.0	21.39	64.9		
Ours-RS		83.52	0.22	15.38	0.48	19.17	14.06	16.12	7.53	72.54	-	89.46	0.43	0.01	73.59	45.61	7.31	-	0.0	0.0	26.2	81.3	+4.81	+16.4
Ours-PH		85.21	0.17	10.85	0.42	19.17	11.2	14.46	40.56	74.63	-	90.31	0.9	0.0	76.86	62.54	30.27	-	0.0	0.0	30.44	82.9	+9.05	+18

Table 3: Domain adaptation results on CS, showing IoU for each class, mean IoU (mIoU), pixel accuracy, mIoU gain and pixel accuracy gain. For each method the first row presents results when trained on the source dataset only, and tested on the target. The second presents results when restyled from the target domain, except from ours, for which the second row shows the configuration GTA(RS-CS) \rightarrow CS, and the third the GTA(PH-CS) \rightarrow CS.

GTA(Cityscapes) \rightarrow Cityscapes

Method	network	road	sidewalk	building	wall	fence	pole	t-light	t-sign	veg	terrain	sky	person	rider	car	truck	bus	train	mbike	bike	mIoU	pix.acc	mIoU gain	pix.acc.gain
FCN in the wild [18]	VGG-16	31.9	18.9	47.7	7.4	3.1	16.0	10.4	1.0	75.5	13.0	58.9	36.0	1.0	67.1	9.5	3.7	0.0	0.0	0.0	21.1	-		
		70.4	32.4	62.1	14.9	5.4	10.9	14.2	2.7	79.2	21.3	64.6	44.1	4.2	70.4	8.0	7.3	0.0	3.5	0.0	27.1	-	+6	
Curriculum [50]	VGG-16	18.1	6.8	64.1	7.3	8.7	21.0	14.9	16.8	45.9	2.4	64.4	41.6	17.5	55.3	8.4	5.0	6.9	4.3	13.8	22.3	-		
		74.9	22.0	71.7	6.0	11.9	8.4	16.3	11.1	75.7	13.3	66.5	38.0	9.3	55.2	18.8	18.9	0.0	16.8	14.6	28.9	-	+6.6	
[38]	VGG-16	73.5	21.3	72.3	18.9	14.3	12.5	15.1	5.3	77.2	17.4	64.3	43.7	12.8	75.4	24.8	7.8	0.0	4.9	1.8	29.6	-		
		88.0	30.5	78.6	25.2	23.5	16.7	23.5	11.6	78.7	27.2	71.9	51.3	19.5	80.4	19.8	18.3	0.9	20.8	18.4	37.1	-	+7.5	
CyCADA [17]	VGG-16	26.0	14.9	65.1	5.5	12.9	8.9	6.0	2.5	70.0	2.9	47.0	24.5	0.0	40.0	12.1	1.5	0.0	0.0	0.0	17.9	54.0		
		85.2	37.2	76.5	21.8	15.0	23.8	22.9	21.5	80.5	31.3	60.7	50.5	9.0	76.9	17.1	28.2	4.5	9.8	0.4	35.4	83.6	+17.5	+29.6
Baseline	VGG-16	73.6	18.4	70.0	9.0	11.4	17.7	7.0	5.2	70.8	7.4	63.6	39.8	1.9	76.2	14.7	3.0	0.0	2.1	0.0	25.9	75.0		
Ours-RS		88.0	32.6	80.0	28.6	20.2	18.7	18.2	8.2	81.0	28.8	77.8	46.9	7.9	79.3	25.4	27.3	1.7	9.6	0.0	35.8	85.9	+9.9	+10.9
Ours-PH		86.3	31.4	80.3	28.2	11.7	22.9	20.	12.8	81.0	26.7	78.4	47.9	11.4	79.1	22.7	17.0	4.0	11.4	0.0	35.5	85.2	+9.6	+10.2
[53]	ResNet-38 [47]	70.0	23.7	67.8	15.4	18.1	40.2	41.9	25.3	78.8	11.7	31.4	62.9	29.8	60.1	21.5	26.8	7.7	28.1	12.0	35.4	-		
		89.6	58.9	78.5	33.0	22.3	41.4	48.2	39.2	83.6	24.3	65.4	49.3	20.2	83.3	39.0	48.6	12.5	20.3	35.3	47.0	-	+11.6	
I2I Adapt [30]	DenseNet [19]	67.3	23.1	69.4	13.9	14.4	21.6	19.2	12.4	78.7	24.5	74.8	49.3	3.7	54.1	8.7	5.3	2.6	6.2	1.9	29.0	-		
		85.8	37.5	80.2	23.3	16.1	23.0	14.5	9.8	79.2	36.5	76.4	53.4	7.4	82.8	19.1	15.7	2.8	13.4	1.7	35.7	-	+6.7	
SG-GAN [25]	PatchGAN[22]																				24.6	54.5		
																					37.4	81.72	+12.8	+27.2
UADA [34]	ResNet-50																				34.8	-		
																					38.2	-	+3.4	
Baseline	ResNet-101	47.9	19.3	66.4	11.8	10.9	23.8	12.4	15.5	79.0	17.3	75.3	53.5	17.4	72.6	6.3	1.8	0.1	16.5	24.9	30.2	66.8		
Ours-RS		90.1	38.1	80.4	15.2	14.5	28.4	13.9	19.9	81.7	31.4	78.4	51.6	18.1	78.0	20.3	22.5	1.4	18.4	38.4	39.0	86.3	+8.8	+19.5
Ours-PH		89.3	47.1	80.3	13.2	13.4	20.1	13.4	19.2	82.5	29.6	77.2	52.3	16.0	80.4	19.0	25.1	1.84	15.0	30.1	38.2	85.9	+8.0	+19.1

Table 4: Domain adaptation results on CS, showing IoU for each class, mean IoU (mIoU), pixel accuracy, mIoU gain and pixel accuracy gain. For each method the first row presents results when trained on the source dataset only, and tested on the target. The second presents results when restyled from the target domain, except from ours, for which the second row shows the configuration GTA(RS-Map) \rightarrow CS, and the third the GTA(PH-Map) \rightarrow CS

GTA(Mapillary) \rightarrow Cityscapes

Method	network	road	sidewalk	building	wall	fence	pole	t-light	t-sign	veg	terrain	sky	person	rider	car	truck	bus	train	mbike	bike	mIoU	pix.acc	mIoU gain	pix.acc.gain
Ours-RS	VGG-16	86.5	29.7	79.4	21.7	13.8	26.8	7.7	2.4	79.5	20.5	70.4	45.7	3.9	78.5	20.7	24.4	4.7	5.6	0.0	32.7	83.9	+6.8	+8.9
Ours-PH		86.1	30.5	77.5	19.3	9.5	20.6	7.3	9.0	79.2	23.2	71.5	46.1	3.0	80.1	22.7	13.5	0.0	5.4	0.0	32.1	84.1	+6.1	+9.1
Ours-RS	ResNet-101	87.5	22.1	80.8	18.8	17.3	15.4	10.0	7.4	81.5	20.3	81.4	50.5	19.5	77.4	26.5	29.3	0.1	16.1	16.6	35.7	86.0	+5.5	+19.2
Ours-PH		87.7	24.6	79.0	16.0	7.9	16.7	7.0	8.9	81.6	27.2	82.3	49.5	13.9	77.3	31.3	38.3	0.5	25.7	18.5	36.5	85.6	+6.3	+18.8

validate and assess our proposed technique, we fix K to 5 for all conducted experiments, which is a good compromise between efficiency and effectiveness.

4.1. Semantic Segmentation

In this section, we present results for data restyling on the semantic segmentation task in a synthetic to-real adaptation setting. We expect that our technique will add important diversity to the virtual source domain and infuse it with

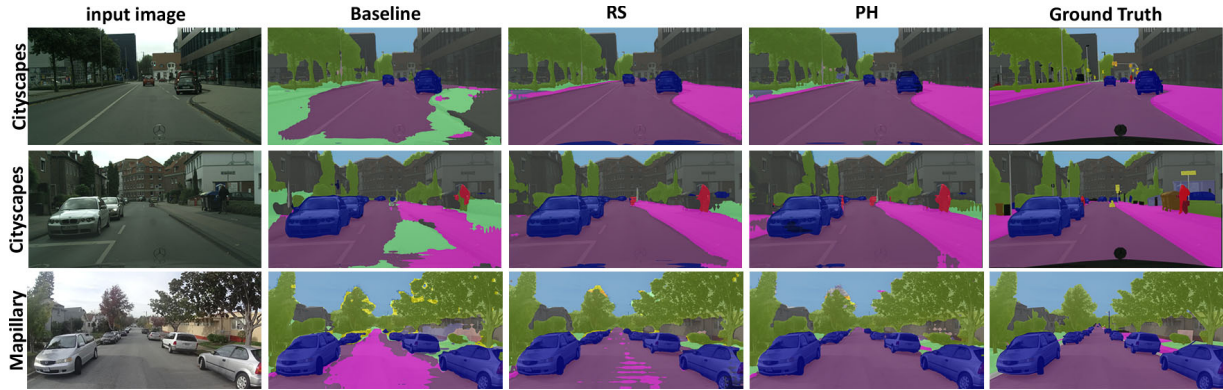


Figure 3: Qualitative results on adaptation from GTA5 to Mapillary and Cityscapes. Rows correspond to predictions for sample images in Cityscapes and Mapillary. From left to right: input image, baseline prediction, ours-RS and ours-PH. Best viewed in color.

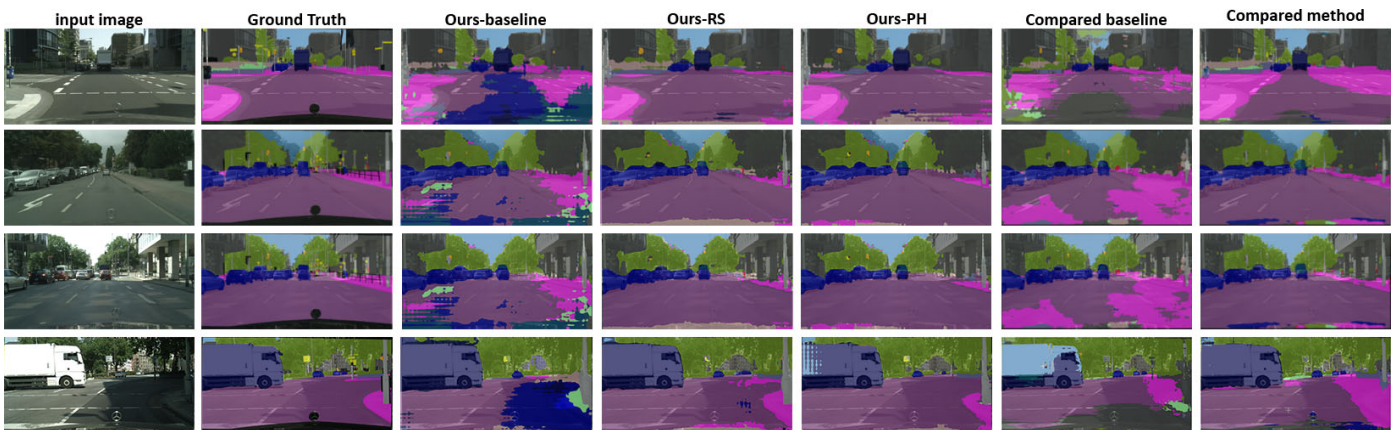


Figure 4: Qualitative results on samples of the Cityscapes dataset, for the semantic segmentation task on different datasets. From left to right: input rgb, our baseline result, our result with random style selection (RS), our result with style selection via perceptual hashing (PH), compared method’s baseline result, and compared method’s result. Each row presents comparison with a different method. From top to bottom: [53], SG-GAN [25], UADA [34], and once more [53].

properties from the real target domain.

We use four datasets, one virtual and three real:

1) Cityscapes, a real-world dataset, capturing street scenes of 50 different cities, totaling 5,000 images with pixel-level labels. The dataset is divided into a training set with 2,975 images, a validation set with 500 images. All images are shot with the same car and camera.

2) GTA, a virtual dataset that contains 24,966 high-resolution images, automatically annotated into 19 classes. The dataset is rendered from the video-game Grand Theft Auto V and is based on the city of Los Angeles with labels fully compatible with those of Cityscapes.

3) Mapillary Vistas, a large-scale street-level image dataset containing 25,000 high-resolution images (split into 18,000 for training, 2,000 for validation, 5,000 for testing; at an average resolution of 9 megapixels). Images are shot in various countries using multiple cameras and their dense labels cover 66 classes.

4) ApolloScope, an open source dataset collected at Beijing in China, including 25 pre-defined semantic classes. Image frames in the dataset are collected every one meter with resolution 3384×2710 . Among all available images, we have kept 8327 frames for evaluation.

We use GTA as our labelled synthetic source data distribution, Mapillary, ApolloScope and Cityscapes for the real domain data distributions, and use the overlapping labels among them. As aforementioned, we enrich the source dataset with our restyled samples and increase its size five-fold.

Our experiments are based on DeepLab-v2 [6] with ResNet-101 [16] and VGG-16 [39] encoders, both initialized with pre-trained weights on ImageNet [10]. All models are trained for 27 epochs using SGD with a learning rate of 2.5×10^{-4} , supported by a 0.9 momentum, a weight decay of 5×10^{-4} and a polynomial learning rate decay policy with $\gamma = 0.9$. Experiments are run using Tensorflow 1.10

[1] and PyTorch 1.1 [32].

Table 1 presents results for GTA(Mapillary) \rightarrow Mapillary in comparison to [34], the only method to presents results in Map, albeit in their case it is considered as unseen. “Unseen” refers to the scenario where a domain adaptation model was trained using a specific target dataset to align its source domain to, but applied to another one, which is similar in context and represents the same domain as the target. It is a challenging scenario that has been lightly addressed in recent work.

We observe that data restyling offers competitive performance and a much larger increase compared to the baseline, with matched restyling (PH) additionally offering a higher boost compared to random selection (RS).

Nonetheless, adapting data from the virtual domain to the real should not be bound to a specific dataset. Whereas the use of unlabeled styles images from the target domain contributes efficiently to domain alignment, we should accord special respect to the case where the target distribution is partly different but of the same context. Owing to the fact that real-life scenarios consist of such cases, it is crucially important for domain adaptation methods and models to adapt properly to new, previously unseen data. Hence, we take a step forward, and evaluate our technique in similar - but unseen - distributions as well.

Table 2 presents results for the conducted GTA(Map) \rightarrow AS experiment. While the synthetic data were restyled using Map’s data distribution, the model’s performance on the AS real – but unseen – data distribution is preserved and surpasses that reported in [34]. As with GTA(Map) \rightarrow Map, a performance increase is observed for PH compared to RS.

Finally, we perform the GTA(CS) \rightarrow CS experiment and present our results in Table 3 which are consistent for both backends used. Since most recent works offer results on CS as well, we can compare our performance to the state-of-the-art. As some methods use different baselines, we report these and then focus on the gain offered by each method and find that our data restyling technique remains competitive with most similar methods. Interestingly, our approach only pre-processes and enriches the data fed to the baseline model, while the compared methods utilize complex training schemes, embed indirect objectives and employ difficult to train GANs.

Curiously, unlike all other experiments, RS performance is higher than PH in CS, which can be attributed to CS’s lack of diversity compared to the other datasets [21]. Table 4 complements this final experiment by presenting results when using Map as the style pool. We find that while performance degrades compared to using the target dataset (CS) as the style domain, there is still a gain when applied to another real data distribution. Notably, the discrepancy be-

tween RS and PH is still different from all other experiments in that no significant increase is observed for PH when targeting CS. Apart from the quantitative evaluation, we also offer a set of exemplary qualitative results for both Map and CS in Figure 3. We additionally offer qualitative results on samples presented by [53, 25, 34] in Figure 4, showcasing the competitiveness of our technique.

Overall, we observe: **i)** that data restyling is competitive to most other compared UDA methods for semantic segmentation, **ii)** an increased generalization performance to unseen distributions, and **iii)** that matching styles helps in addressing the performance deterioration that uncanny restyles via random matching would introduce.

4.2. Depth Regression

We conduct a final experiment on a dense regression task, monocular depth estimation, an ill-posed problem that is furthermore very difficult to collect high quality labelled data. Hence, using synthetic data generation is a very promising approach, constituting synthetic-to-real adaptation very relevant.

We use the recently released 360D dataset [52] that was generated via rendering synthetic, as well as realistic scanned scenes. It comprises 360° renders of existing 3D datasets, annotated with their corresponding ground truth depth maps. It is composed of omnidirectional renders from Matterport3D (*M3D*) [5], Stanford2D3D (*S2D3D*) [2] and SunCG [40] (*SunCG*). While the first two contain scanned 3D textured models of real indoors spaces, the third is composed of Computer Generated (synthetic) scenes only. In addition, the SUN360 [48] dataset contains a very large variety of only color images, depicting real world scenes and captured with real 360° cameras. Given that the context of 360D is indoors scenes, we only use that subset of Sun360 for deriving realistic styles that consists of 33512 samples.

We use the synthetic SunCG dataset as our source domain and the realistic Sun360 dataset as our style pool. We train RectNet [52] only on the valid subset of SunCG (4716 samples) and consider it as our baseline. We follow the same training and data validity schemes as in [52].

Given that Sun360 does not offer ground truth depth measurements we offer qualitative results of the baseline and domain adapted networks in Figure 5. It is evident that visually performance increases when applied to the unlabelled Sun360 domain directly. In order to present quantitative results we also evaluate our trained models in an unseen task, i.e. SunCG(Sun360) \rightarrow S2D3D-M3D using the realistic S2D3D-M3D data. In addition, we restyle the S2D3D-M3D data using the Sun360 style pool in order to infuse its style into the ground truth paired S2D3D-M3D data and be able to calculate quantifiable results. We refer to this task as SunCG(Sun360) \rightarrow RS-S2D3D-M3D.

Quantitative results are presented in Table 5, for which

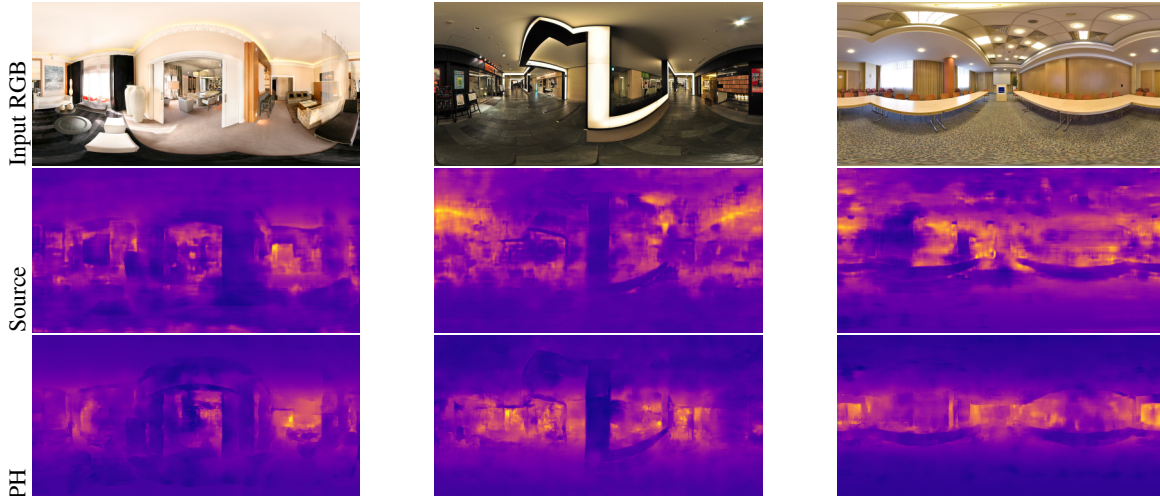


Figure 5: Qualitative results on omnidirectional dense depth estimation on samples of SUN360 where there is no ground truth depth map available.

Table 5: Results of omnidirectional depth estimation for the different domain adaptation scenarios (\downarrow means lower is better, and \uparrow means higher is better). The first three rows represent evaluating on M3D and S2D3D datasets, while the latter two correspond to evaluations on the RS-M3D-S2D3D with styles derived from SUN360. Baseline implies that RectNet was trained on SunCG only, ours-RS that RectNet was trained on RS-SunCG, while ours-PH that RectNet was trained with PH-SunCG with styles from SUN360.

Method	Abs. Rel. \downarrow	Sq. Rel. \downarrow	RMSE \downarrow	RMSE (log) \downarrow	$\delta < 1.25 \uparrow$	$\delta < 1.25^2 \uparrow$	$\delta < 1.25^3 \uparrow$
Baseline	0.233	0.204	0.669	0.283	0.614	0.891	0.966
Ours-RS	0.268	0.306	0.757	0.321	0.626	0.856	0.938
Ours-PH	0.209	0.188	0.622	0.261	0.693	0.9	0.964
Baseline	0.406	0.511	1.025	0.472	0.371	0.659	0.839
Ours-RS	0.264	0.287	0.747	0.318	0.626	0.857	0.936
Ours-PH	0.231	0.229	0.681	0.285	0.666	0.884	0.956

we used typical metrics as reported in [52]. The results further support previous findings in that restyling the data increases performance to both the targeted domain (RS-S2D3D-M3D), as well as similar domains (S2D3D-M3D), with the largest performance gained obtained on the domain that the styles were picked from. We also find that the matched sample selection strategy helps in increasing domain adaptation performance compared to a random selection.

5. Conclusion

We have shown that explicit data restyling can be an easy to implement, scalable and effective technique for UDA. Besides offering a straightforward way to avoid the complexity of adversarial based and cycle consistency based domain adaptation, it is also ripe for experimentation in

conjunction with traditional methods, as it is purely a data pre-processing step. However, it is because to this reason alone that it is much more applicable and, due to its inherently parallel nature, scales extremely well. It poses as a very practical tool to adapt models when it is easy to obtain large quantities of unlabelled data (e.g. industrial/production settings). Given the generality of the proposed technique, it was validated in different vision tasks and datasets, and found to be a promising alternative to most approaches found in the literature, whilst not being task or dataset constrained.

References

- [1] M. Abadi, A. Agarwal, P. Barham, E. Brevdo, Z. Chen, C. Citro, G. S. Corrado, A. Davis, J. Dean, M. Devin, S. Ghemawat, I. Goodfellow, A. Harp, G. Irving, M. Isard, Y. Jia,

- R. Jozefowicz, L. Kaiser, M. Kudlur, J. Levenberg, D. Mane, R. Monga, S. Moore, D. Murray, C. Olah, M. Schuster, J. Shlens, B. Steiner, I. Sutskever, K. Talwar, P. Tucker, V. Vanhoucke, V. Vasudevan, F. Viegas, O. Vinyals, P. Warden, M. Wattenberg, M. Wicke, Y. Yu, and X. Zheng. TensorFlow: Large-Scale Machine Learning on Heterogeneous Distributed Systems. Mar. 2016. 7
- [2] I. Armeni, S. Sax, A. R. Zamir, and S. Savarese. Joint 2d-3d-semantic data for indoor scene understanding. *CoRR*, abs/1702.01105, 2017. 7
- [3] A. Atapour-Abarghouei and T. P. Breckon. Real-time monocular depth estimation using synthetic data with domain adaptation via image style transfer. In *Proceedings of the IEEE Conference on Computer Vision and Pattern Recognition*, volume 18, page 1, 2018. 2, 3
- [4] K. Bousmalis, N. Silberman, D. Dohan, D. Erhan, and D. Krishnan. Unsupervised pixel-level domain adaptation with generative adversarial networks. In *The IEEE Conference on Computer Vision and Pattern Recognition (CVPR)*, volume 1, page 7, 2017. 2
- [5] A. Chang, A. Dai, T. Funkhouser, M. Halber, M. Niessner, M. Savva, S. Song, A. Zeng, and Y. Zhang. Matterport3D: Learning from RGB-D data in indoor environments. *International Conference on 3D Vision (3DV)*, 2017. 7
- [6] L.-C. Chen, G. Papandreou, I. Kokkinos, K. Murphy, and A. L. Yuille. Deeplab: Semantic image segmentation with deep convolutional nets, atrous convolution, and fully connected crfs. In *IEEE Transactions on Pattern Analysis and Machine Intelligence*, volume PP, 06 2016. 6
- [7] Y.-H. Chen, W.-Y. Chen, Y.-T. Chen, B.-C. Tsai, Y.-C. F. Wang, and M. Sun. No more discrimination: Cross city adaptation of road scene segmenters. In *Computer Vision (ICCV), 2017 IEEE International Conference on*, pages 2011–2020. IEEE, 2017. 3
- [8] M. Cordts, M. Omran, S. Ramos, T. Rehfeld, M. Enzweiler, R. Benenson, U. Franke, S. Roth, and B. Schiele. The cityscapes dataset for semantic urban scene understanding. In *2016 IEEE Conference on Computer Vision and Pattern Recognition (CVPR)*, pages 3213–3223, 2016. 3
- [9] T. Dao, A. Gu, A. Ratner, V. Smith, C. D. Sa, and C. Ré. A kernel theory of modern data augmentation. In *Proceedings of the 36th International Conference on Machine Learning, ICML 2019, 9-15 June 2019, Long Beach, California, USA*, pages 1528–1537, 2019. 4
- [10] J. Deng, W. Dong, R. Socher, L. jia Li, K. Li, and L. Fei-fei. Imagenet: A large-scale hierarchical image database. In *In CVPR*, 2009. 6
- [11] A. Gaidon, Q. Wang, Y. Cabon, and E. Vig. Virtual worlds as proxy for multi-object tracking analysis. In *Proceedings of the IEEE conference on computer vision and pattern recognition*, pages 4340–4349, 2016. 2
- [12] Y. Ganin and V. Lempitsky. Unsupervised domain adaptation by backpropagation. In *Proceedings of the 32nd International Conference on International Conference on Machine Learning - Volume 37*, pages 1180–1189. JMLR. org, 2015. 2
- [13] Y. Ganin, E. Ustinova, H. Ajakan, P. Germain, H. Larochelle, F. Laviolette, M. Marchand, and V. Lempitsky. Domain-adversarial training of neural networks. *J. Mach. Learn. Res.*, 17(1):2096–2030, Jan. 2016. 2
- [14] L. A. Gatys, A. S. Ecker, and M. Bethge. A neural algorithm of artistic style. volume abs/1508.06576, 2015. 2, 3
- [15] I. Goodfellow, J. Pouget-Abadie, M. Mirza, B. Xu, D. Warde-Farley, S. Ozair, A. Courville, and Y. Bengio. Generative adversarial nets. In *Advances in neural information processing systems*, pages 2672–2680, 2014. 2
- [16] K. He, X. Zhang, S. Ren, and J. Sun. Deep residual learning for image recognition. In *2016 IEEE Conference on Computer Vision and Pattern Recognition, CVPR 2016, Las Vegas, NV, USA, June 27-30, 2016*, pages 770–778, 2016. 6
- [17] J. Hoffman, E. Tzeng, T. Park, J.-Y. Zhu, P. Isola, K. Saenko, A. A. Efros, and T. Darrell. Cycada: Cycle-consistent adversarial domain adaptation. In *ICML*, 2018. 3, 5
- [18] J. Hoffman, D. Wang, F. Yu, and T. Darrell. Fcns in the wild: Pixel-level adversarial and constraint-based adaptation. In *CoRR*, volume abs/1612.02649, 2016. 2, 5
- [19] G. Huang, Z. Liu, L. van der Maaten, and K. Q. Weinberger. Densely connected convolutional networks. *2017 IEEE Conference on Computer Vision and Pattern Recognition (CVPR)*, pages 2261–2269, 2017. 5
- [20] G. Huang, Y. Sun, Z. Liu, D. Sedra, and K. Q. Weinberger. Deep networks with stochastic depth. In *European Conference on Computer Vision*, pages 646–661. Springer, 2016. 1
- [21] X. Huang, X. Cheng, Q. Geng, B. Cao, D. Zhou, P. Wang, Y. Lin, and R. Yang. The ApolloScape dataset for autonomous driving. In *2018 IEEE/CVF Conference on Computer Vision and Pattern Recognition Workshops (CVPRW)*. IEEE, jun 2018. 3, 7
- [22] P. Isola, J.-Y. Zhu, T. Zhou, and A. A. Efros. Image-to-image translation with conditional adversarial networks. In *2017 IEEE Conference on Computer Vision and Pattern Recognition (CVPR)*, pages 5967–5976, 2017. 5
- [23] P. T. Jackson, A. Atapour-Abarghouei, S. Bonner, T. P. Breckon, and B. Obara. Style augmentation: Data augmentation via style randomization. In *The IEEE Conference on Computer Vision and Pattern Recognition (CVPR) Workshops*, June 2019. 3
- [24] Y. Lecun, L. Bottou, Y. Bengio, and P. Haffner. Gradient-based learning applied to document recognition. In *Proceedings of the IEEE*, pages 2278–2324, 1998. 2
- [25] P. Li, X. Liang, D. Jia, and E. Xing. Semantic-aware gradgan for virtual-to-real urban scene adaptation. In *British Machine Vision Conference 2018, BMVC 2018, Northumbria University, Newcastle, UK, September 3-6, 2018*, page 73, 2018. 3, 5, 6, 7
- [26] Y. Li, M. Liu, X. Li, M. Yang, and J. Kautz. A closed-form solution to photorealistic image stylization. In *Computer Vision - ECCV 2018 - 15th European Conference, Munich, Germany, September 8-14, 2018, Proceedings, Part III*, pages 468–483, 2018. 4
- [27] M.-Y. Liu and O. Tuzel. Coupled generative adversarial networks. In *NIPS*, 2016. 2
- [28] J. Long, E. Shelhamer, and T. Darrell. Fully convolutional networks for semantic segmentation. In *IEEE Conference*

- on *Computer Vision and Pattern Recognition, CVPR 2015, Boston, MA, USA, June 7-12, 2015*, pages 3431–3440, 2015. 3
- [29] M. Menze and A. Geiger. Object scene flow for autonomous vehicles. In *Proceedings of the IEEE Conference on Computer Vision and Pattern Recognition*, pages 3061–3070, 2015. 3
- [30] Z. Murez, S. Kolouri, D. J. Kriegman, R. Ramamoorthi, and K. Kim. Image to image translation for domain adaptation. In *2018 IEEE Conference on Computer Vision and Pattern Recognition, CVPR 2018, Salt Lake City, UT, USA, June 18-22, 2018*, pages 4500–4509, 2018. 3, 5
- [31] G. Neuhold, T. Ollmann, S. Rota Bulò, and P. Kotschieder. The mapillary vistas dataset for semantic understanding of street scenes. In *The IEEE International Conference on Computer Vision (ICCV)*, Oct 2017. 3
- [32] A. Paszke, S. Gross, S. Chintala, G. Chanan, E. Yang, Z. DeVito, Z. Lin, A. Desmaison, L. Antiga, and A. Lerer. Automatic differentiation in pytorch. 2017. 7
- [33] S. R. Richter, V. Vineet, S. Roth, and V. Koltun. Playing for data: Ground truth from computer games. In *ECCV*, 2016. 2, 3
- [34] R. Romijnders, P. Meletis, and G. Dubbelman. A domain agnostic normalization layer for unsupervised adversarial domain adaptation. In *IEEE Winter Conference on Applications of Computer Vision, WACV 2019, Waikoloa Village, HI, USA, January 7-11, 2019*, pages 1866–1875, 2019. 3, 5, 6, 7
- [35] G. Ros, L. Sellart, J. Materzynska, D. Vazquez, and A. M. Lopez. The synthia dataset: A large collection of synthetic images for semantic segmentation of urban scenes. In *The IEEE Conference on Computer Vision and Pattern Recognition (CVPR)*, June 2016. 3
- [36] K. Saenko, B. Kulis, M. Fritz, and T. Darrell. Adapting visual category models to new domains. In *European conference on computer vision*, pages 213–226. Springer, 2010. 2
- [37] K. Saito, Y. Ushiku, T. Harada, and K. Saenko. Adversarial dropout regularization. In *International Conference on Learning Representations*, 2018. 3
- [38] S. Sankaranarayanan, Y. Balaji, A. Jain, S. N. Lim, and R. Chellappa. Learning from synthetic data: Addressing domain shift for semantic segmentation. In *The IEEE Conference on Computer Vision and Pattern Recognition (CVPR)*, 2018. 2, 3, 5
- [39] K. Simonyan and A. Zisserman. Very deep convolutional networks for large-scale image recognition. In *International Conference on Learning Representations*, 2015. 6
- [40] S. Song, F. Yu, A. Zeng, A. X. Chang, M. Savva, and T. Funkhouser. Semantic scene completion from a single depth image. *IEEE Conference on Computer Vision and Pattern Recognition*, 2017. 7
- [41] N. Srivastava, G. Hinton, A. Krizhevsky, I. Sutskever, and R. Salakhutdinov. Dropout: a simple way to prevent neural networks from overfitting. *The Journal of Machine Learning Research*, 15(1):1929–1958, 2014. 1
- [42] G. J. Stein and N. Roy. Genesis-rt: Generating synthetic images for training secondary real-world tasks. In *2018 IEEE International Conference on Robotics and Automation (ICRA)*, pages 7151–7158. IEEE, 2018. 2
- [43] C. Thomas and A. Kovashka. Artistic object recognition by unsupervised style adaptation. In C. V. Jawahar, H. Li, G. Mori, and K. Schindler, editors, *Computer Vision – ACCV 2018*, pages 460–476, Cham, 2019. Springer International Publishing. 3
- [44] A. Torralba and A. A. Efros. Unbiased look at dataset bias. In *Computer Vision and Pattern Recognition (CVPR), 2011 IEEE Conference on*, pages 1521–1528. IEEE, 2011. 2
- [45] Y.-H. Tsai, W.-C. Hung, S. Schulter, K. Sohn, M.-H. Yang, and M. Chandraker. Learning to adapt structured output space for semantic segmentation. In *The IEEE Conference on Computer Vision and Pattern Recognition (CVPR)*, June 2018. 3
- [46] X. Wang, K. Pang, X. Zhou, Y. Zhou, L. Li, and J. Xue. A visual model-based perceptual image hash for content authentication. volume 10, pages 1336–1349, 2015. 4
- [47] Z. Wu, C. Shen, and A. van den Hengel. Wider or deeper: Revisiting the resnet model for visual recognition. In *CoRR*, volume abs/1611.10080, 2019. 5
- [48] J. Xiao, K. A. Ehinger, A. Oliva, and A. Torralba. Recognizing scene viewpoint using panoramic place representation. In *Computer Vision and Pattern Recognition (CVPR), 2012 IEEE Conference on*, pages 2695–2702. IEEE, 2012. 7
- [49] J. Yosinski, J. Clune, Y. Bengio, and H. Lipson. How transferable are features in deep neural networks? In *Advances in neural information processing systems*, pages 3320–3328, 2014. 2
- [50] Y. Zhang, P. David, and B. Gong. Curriculum domain adaptation for semantic segmentation of urban scenes. In *The IEEE International Conference on Computer Vision (ICCV)*, volume 2, page 6, 2017. 2, 3, 5
- [51] J.-Y. Zhu, T. Park, P. Isola, and A. A. Efros. Unpaired image-to-image translation using cycle-consistent adversarial networks. In *Computer Vision (ICCV), 2017 IEEE International Conference on*, 2017. 3
- [52] N. Ziouli, A. Karakottas, D. Zarpalas, and P. Daras. Omnidepth: Dense depth estimation for indoors spherical panoramas. In *The European Conference on Computer Vision (ECCV)*, September 2018. 7, 8
- [53] Y. Zou, Z. Yu, B. Vijaya Kumar, and J. Wang. Unsupervised domain adaptation for semantic segmentation via class-balanced self-training. In *The European Conference on Computer Vision (ECCV)*, September 2018. 3, 5, 6, 7